

Electronic Supplementary Information (ESI†)

for

**Engineered Design of Theranostic Upconversion Nanoparticles
for Tri-modal Upconversion Luminescence/ Magnetic
Resonance/ X-ray Computed Tomography Imaging and
Targeted Delivery of Combined Anticancer Drugs.**

Gan Tian^{a,b}, Wenyan Yin^b, Junjiang Jin^b, Xiao Zhang^{b,c}, Gengmei Xing^b, Shoujian Li^a,
Zhanjun Gu^{*,b} and Yuliang Zhao^{*,a,b,c}

^a College of Chemistry, Sichuan University, Chengdu, 610064, P. R. China

^b Key Laboratory for Biomedical Effects of Nanomaterials and Nanosafety, Institute
of High Energy Physics, Chinese Academy of Sciences, Beijing, 100049, P. R. China

^c Key Laboratory for Biomedical Effects of Nanomaterials and Nanosafety, National
Center for Nanosciences and Technology of China, Beijing, 100190, China

*Corresponding Authors: zjgu@ihep.ac.cn, zhaoyuliang@ihep.ac.cn

Contents: Figure S1-S12 and Table S1-S2

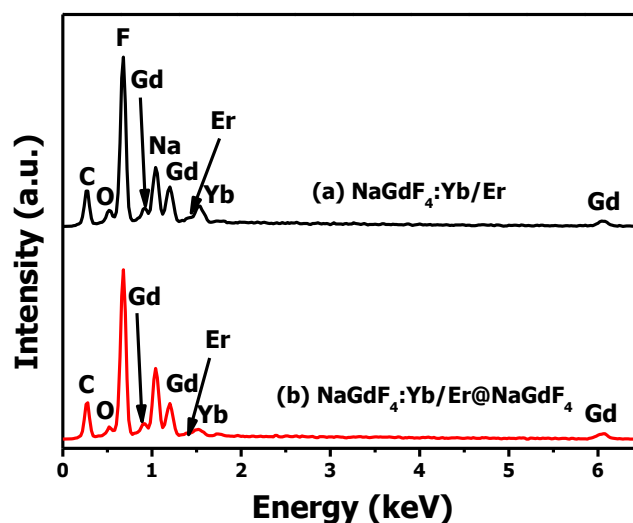


Figure S1. Element composition analysis. EDX spectrum of core-only NaGdF₄:Yb/Er and core-shell structured NaGdF₄:Yb/Er@NaGdF₄ upconversion nanoparticles. From the two curves, we could find that the relative signal intensity ratio Yb/Gd in curve (b) was much weaker than that in curve (a), demonstrating the increase of the Gd content after core-shell fabrication process and confirming the formation of NaGdF₄ shell.

Table S1 Elemental analysis of core and core-shell UCNPs by ICP-MS

Sample	Gd [mol%]	Yb [mol%]	Er [mol%]
NaGdF ₄ :Yb/Er	78.57	19.41	2.02
NaGdF ₄ :Yb/Er@NaGdF ₄	86.94	11.84	1.22

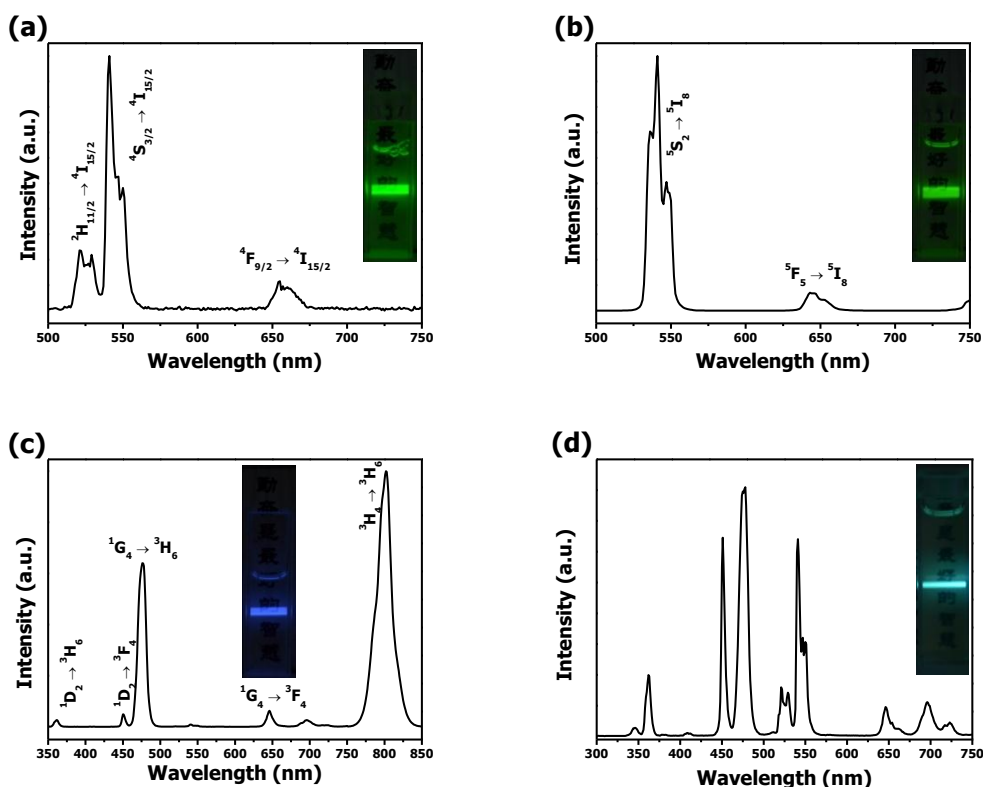


Figure S2. Multicolor upconversion luminescence property. Upconversion emission spectrum and photographs of (a) NaGdF₄:Yb/Er (20/2 mol%), (b) NaGdF₄:Yb/Ho (20/0.5 mol%), (c) NaGdF₄:Yb/Tm (20/0.2 mol%) and (d) NaGdF₄:Yb/Tm,Er (20/0.5/0.2 mol%) in cyclohexane (1 mg/mL) following excitation with 980-nm laser (power: 500 mW), respectively. All emission bands are correspondingly marked with their characteristic energy level transitions.

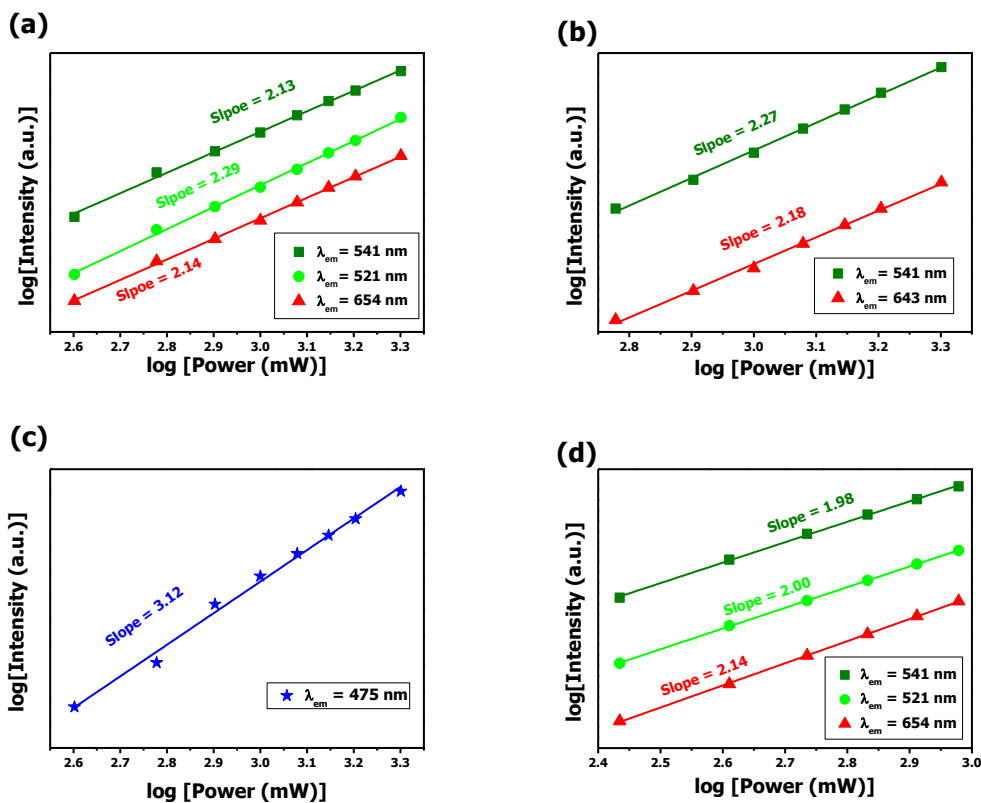


Figure S3. UC mechanism investigation. The Log-Log plots of the UC luminescence intensity versus excitation power for (a) NaGdF₄:Yb/Er (20/2 mol%), (b) NaGdF₄:Yb/Ho (20/0.5 mol%), (c) NaGdF₄:Yb/Tm (20/0.2 mol%) and (d) core-shell NaGdF₄: Yb/Er (20/2 mol%)@NaGdF₄, respectively.

To further reveal the UC mechanism, the pumping power dependence of the emission intensity was investigated. For an unsaturated UC process, the emission intensity (I_f) will be proportional to some power (n) of the infrared excitation (P) power: $I_f \propto P^n$, Where n is the number of infrared photons absorbed per visible photon emitted and it can be calculated from the slope of the Log-Log plots of the UC luminescence intensity versus excitation power. **Figure S3** shows the power dependence of the UC emission intensities and indicates two or three pumping photons are involved for the upconversion process.

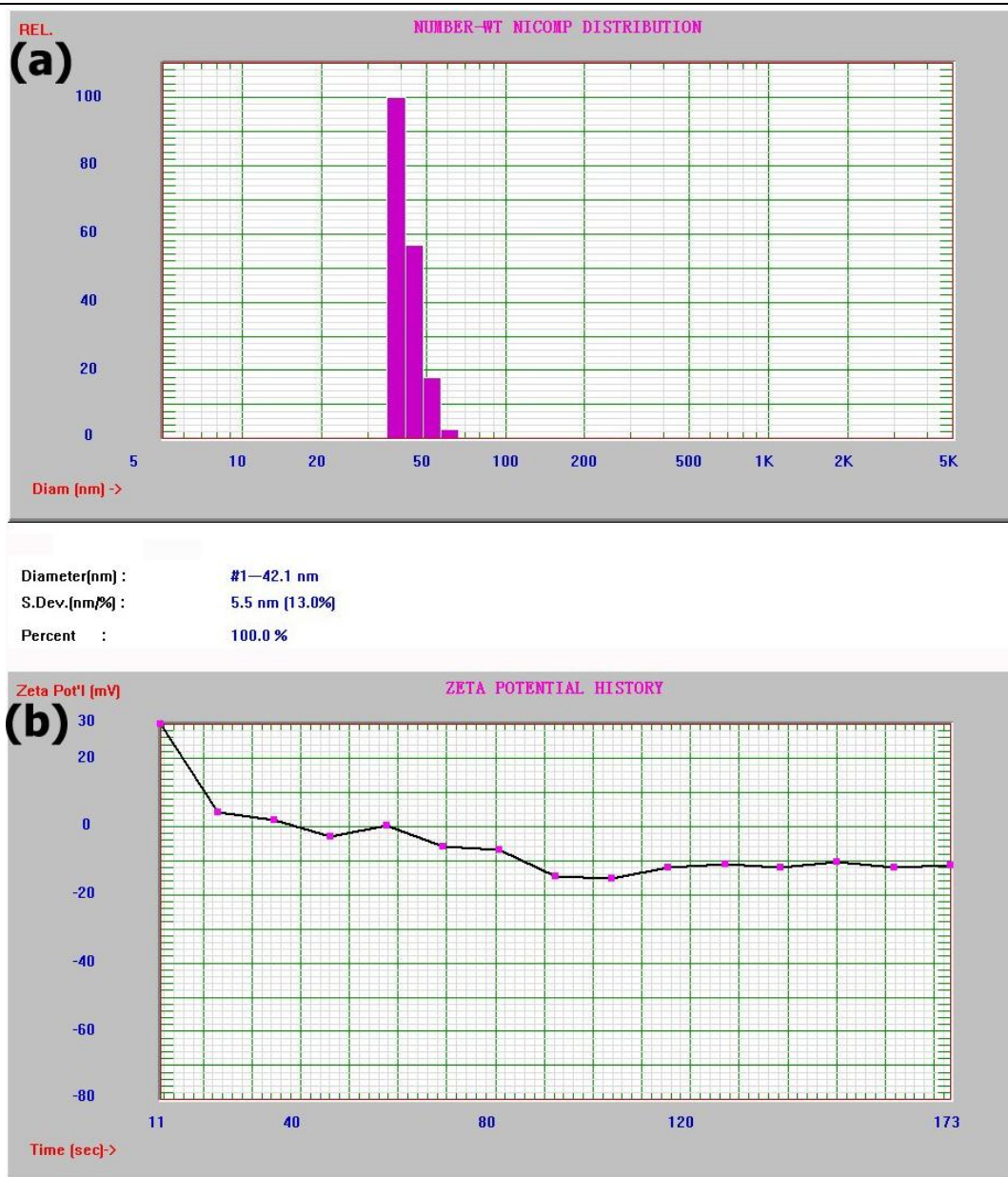


Figure S4. DLS and zeta potential (ζ) analysis of tween-UCNPs dispersed in DI water.

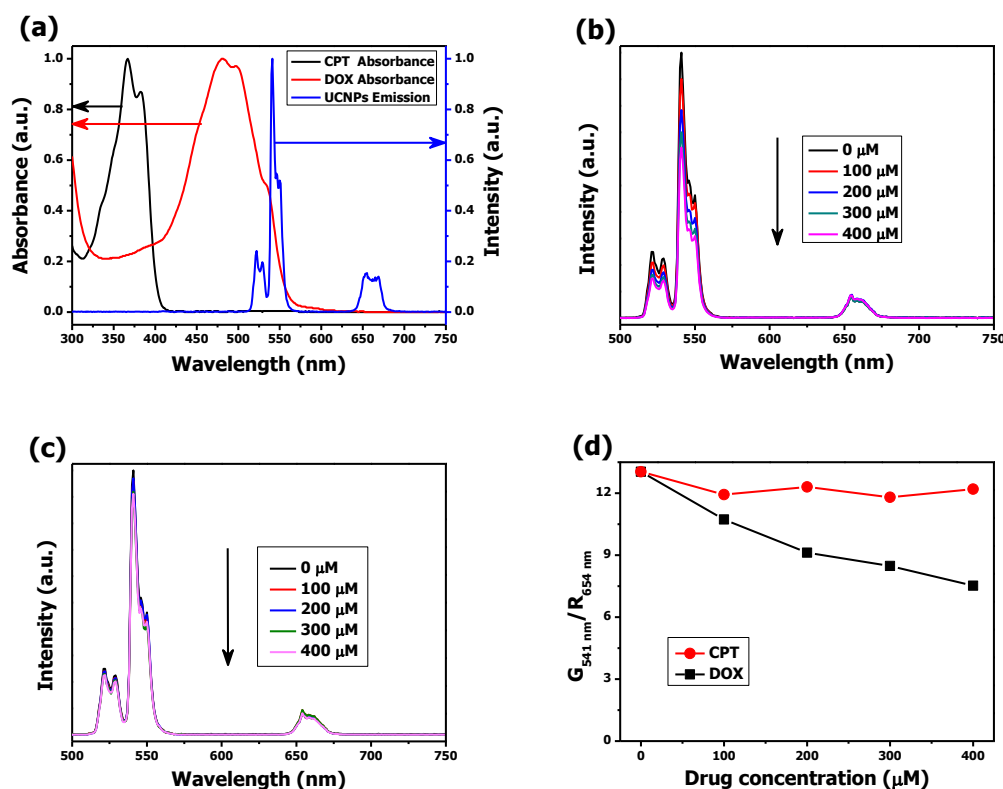


Figure S5. UCL spectrum changes after drug loading. (a) UV-vis absorption spectra of CPT (black) and DOX (red), respectively, and upconversion emission spectrum of UCNPs (blue), From which we could find that the absorption spectra of DOX partly overlaps the green band of the Upconversion emission spectrum from UCNPs, while CPT does not, indicating that the DOX loading should obviously quench the emission intensity due to the possible occurrence of FRET from UCNPs to DOX, whereas CPT loading would not bring significant impact on the spectrum. **Figure S5b** and **Figure S5c** represented the upconversion spectrum of tween-UCNPs after introducing different amount of DOX and CPT, respectively (dispersion: 0.5 mg/mL, power: 500 mW). In combination with the variation tendency of $G_{541\text{ nm}}/R_{654\text{ nm}}$ curves in **Figure S5d**, we could confirm the above deduction.

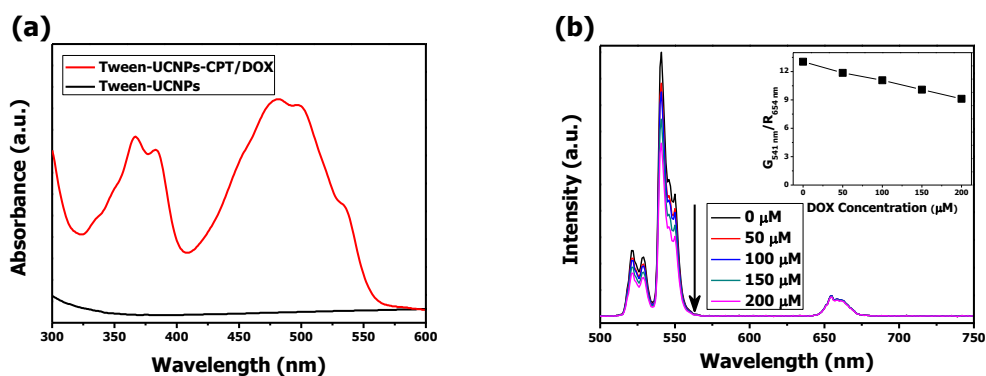


Figure S6. Optical spectra study for drug co-delivery. (a) UV-vis spectra of tween-UCNPs before and after loading of CPT and DOX. (b) Upconversion emission spectra of tween-UCNPs-CPT/DOX under different DOX loading concentration (inset: $G_{541\text{nm}}/R_{654\text{nm}}$ curve).

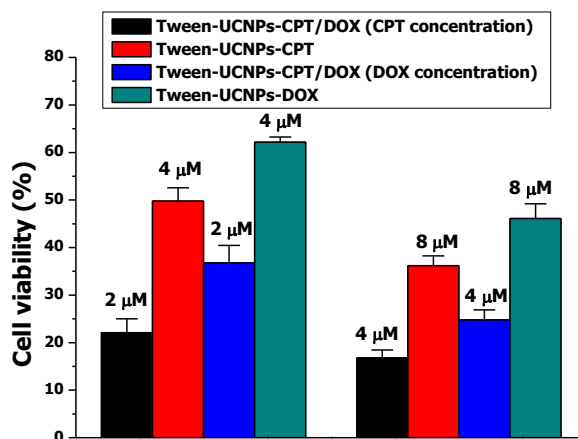


Figure S7. Cytotoxicity data extracted from **Figure 5** in the manuscript for comparison to reflect the synergistic effect in the dual-drug delivery system.

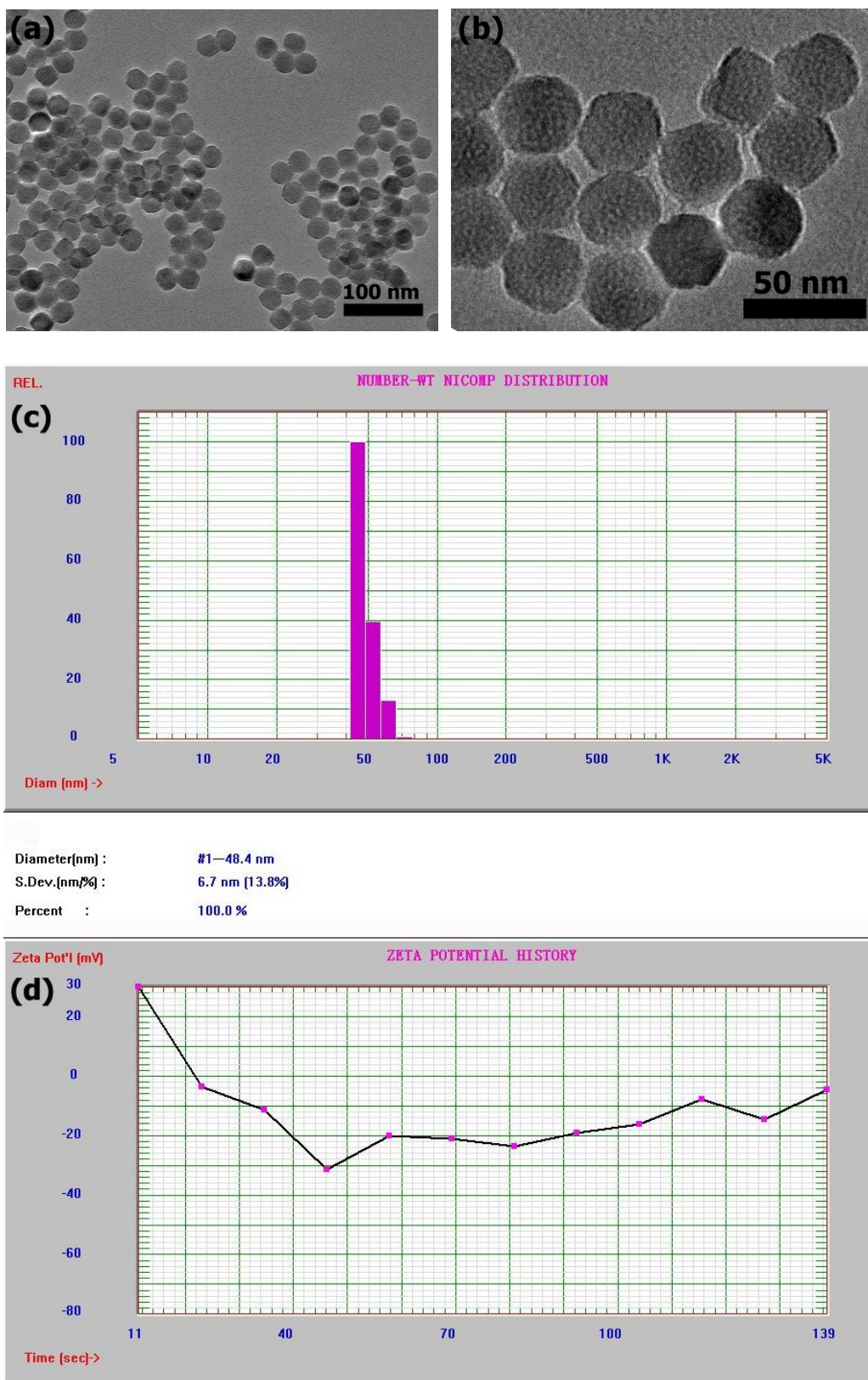


Figure S8. (a, b) TEM images of FA-UCNPs; (c) DLS and (d) zeta potential (ζ) analysis of FA-UCNPs dispersed in DI water.

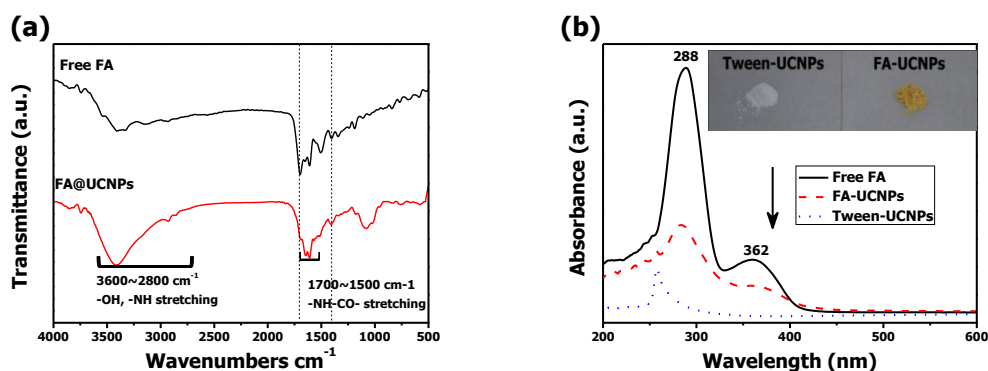


Figure S9. FA attachment confirmation. (a) FT-IR spectrum of free folic acid and FA-conjugated UCNPs; FA molecules were covalently conjugated to tween-UCNPs via amidation mediated by the reaction between $-\text{NH}_2$ group in FA and $-\text{COOH}$ group on the tween-UCNPs. In the spectrum of FA-UCNPs, the peaks between $1500\sim 1700\text{ cm}^{-1}$ attributed to the $-\text{NH-CO-}$ group stretching vibration indicated the successful amidation. (b) UV-vis spectra of free FA, FA-UCNPs and tween-UCNPs dissolved in DMSO. Free FA showed two characteristic absorption peaks at 288 and 362 nm, respectively, and FA-UCNPs also exhibited obvious absorbance signals at the same wavelengths, while tween-UCNPs showed no detectable signals at the two wavelengths, implying FA were, to some extent, covalently conjugated to the UCNPs surface. In addition, the color change between before and after FA conjugation also supported the above conclusion.

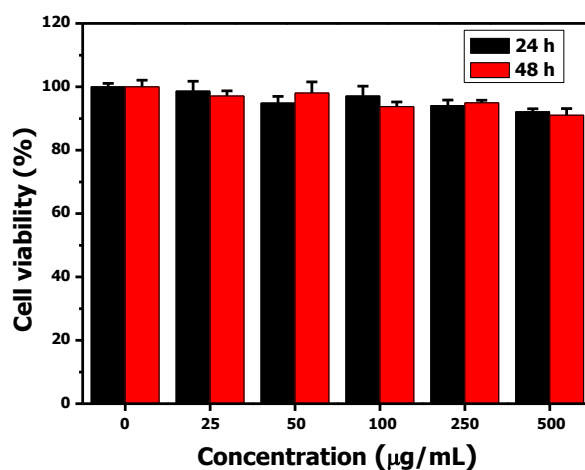


Figure S10. Cell viability studies of HeLa cells by CCK-8 assay after incubation with different concentrations of FA-UCNPs for 24 h and 48 h, respectively.

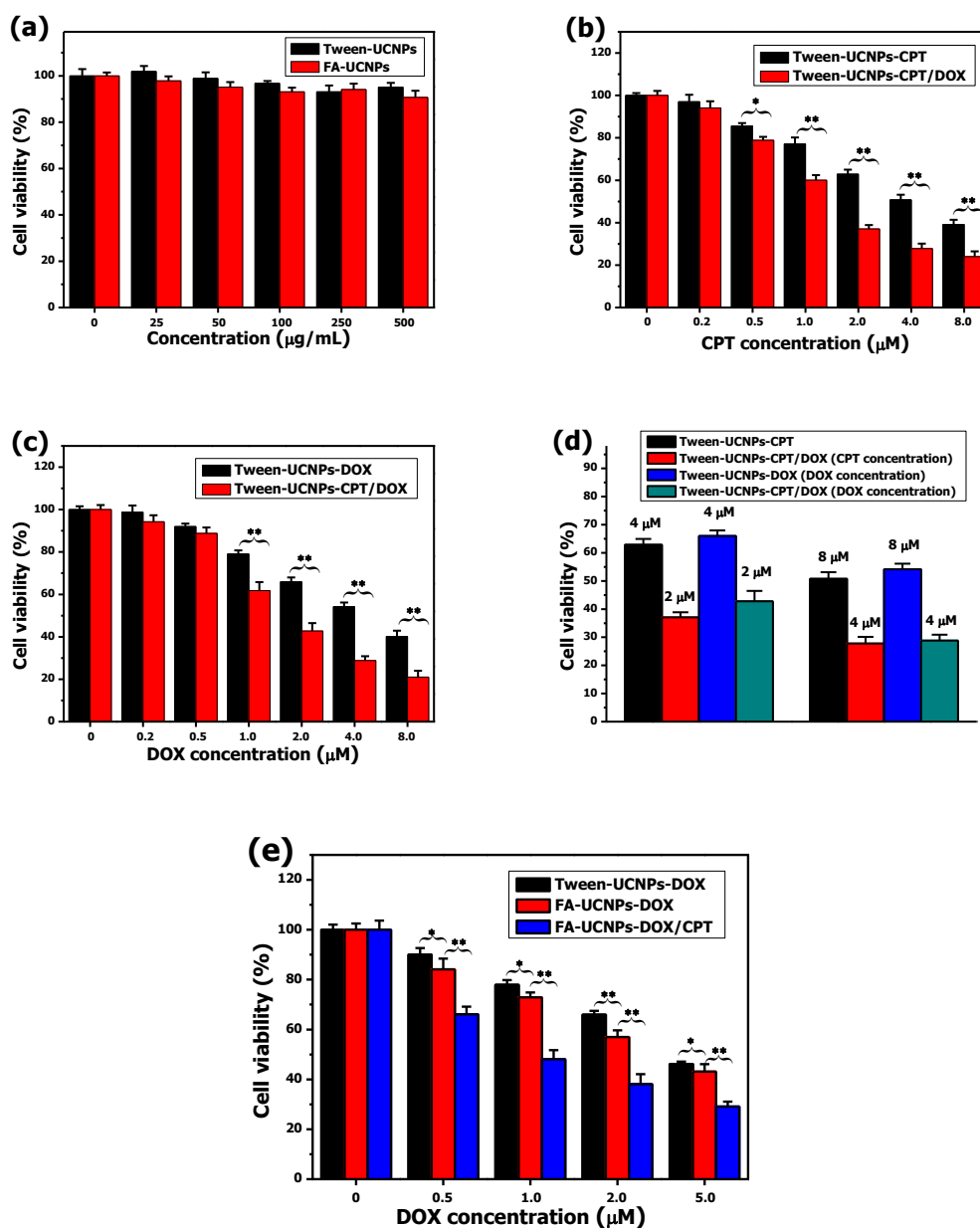
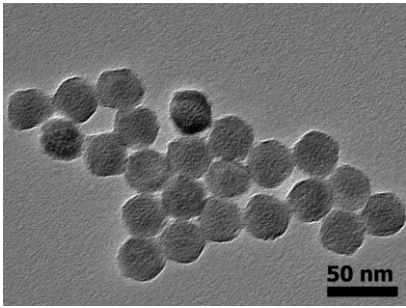
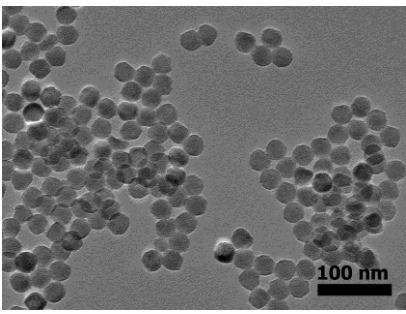


Figure S11. (a) Cytotoxicity estimation against A-549 cancer cells incubated with tween-UCNPs and FA-UCNPs at different concentrations for 24 h, respectively. Cell viability of A-549 cells was still higher than 90 % even treated with a high dosage at 500 $\mu\text{g/mL}$, indicating the tween-UCNPs or FA-UCNPs had low toxicity towards A-549 cells. Cell viability of A-549 cells after treatment with (b) tween-UCNPs-CPT and tween-UCNPs-CPT/DOX, (c) tween-UCNPs-DOX and tween-UCNPs-CPT/DOX respectively. (d) Cytotoxicity data extracted from (b, c) for comparison to reflect the

synergistic effect in the dual-drug delivery system. Results presented in (b-d) demonstrated the higher efficiency and synergistic effect of the dual-drug delivery system. (e) Concentration-dependent cell survival data of A-549 cells treated with tween-UCNPs-DOX, FA-UCNPs-DOX and FA-UCNPs-CPT/DOX, respectively. FR-mediated targeted delivery for A-549 was not so obvious compared with the results for HeLa cells, which could be explained by that the amount of folate receptors produced by A-549 were much fewer than HeLa. $*P < 0.05$; $**P < 0.01$. Error bars were based on six samples.

Table S2. TEM images, hydrodynamic diameter and zeta-potential analysis data for tween-UCNPs and FA-UCNPs.

Samples	TEM image	hydrodynamic diameter (nm)	zeta-potential (mV)
tween-UCNPs		42.1 ± 5.5	-9.65 ± 0.72
FA-UCNPs		48.4 ± 6.7	-15.75 ± 2.11

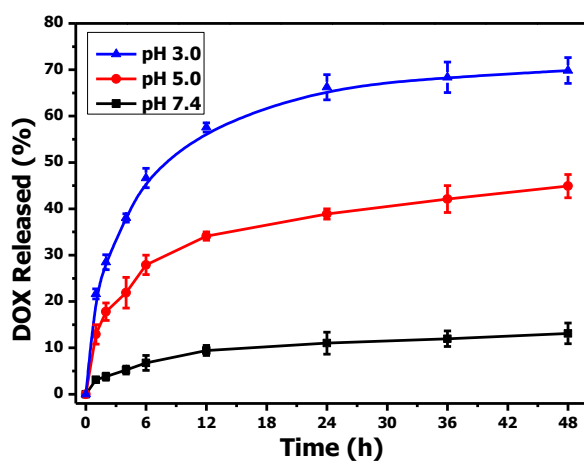


Figure S12. DOX release curves at different pH values. Lowering pH value benefits the DOX release and about 70 % DOX was detached from the tween-UCNPs at pH 3.0.